
Deep Geometric Moment

Rajhans Singh
rsingh70@asu.edu

Ankita Shukla
ashukl20@asu.edu

Pavan Turaga
pturaga@asu.edu

School of Arts, Media and Engineering
School of Electrical, Computer, and Energy Engineering
Arizona State University
Tempe, AZ 85281

Abstract

Deep networks for image classification often rely more on texture information than object shape. While efforts have been made to make deep-models shape-aware, it is often difficult to make such models simple, interpretable, or rooted in known mathematical definitions of shape. This paper presents a deep-learning model inspired by geometric moments, a classically well understood approach to measure shape-related properties. The proposed method consists of a trainable network for generating coordinate bases and affine parameters for making the features geometrically invariant, yet in a task-specific manner. The proposed model improves the final feature’s interpretation. We demonstrate the effectiveness of our method on standard image classification datasets. The proposed model achieves higher classification performance as compared to the baseline and standard ResNet models while substantially improving interpretability.

1 Introduction

Advances in deep learning have resulted in state-of-the-art performance for a wide variety of computer vision tasks. The large quantity of training data and high computation resources have made convolutional neural networks (CNN) into a common backbone model for many tasks; including image classification [27, 37, 16], object detection [12, 31, 15], segmentation [32, 3, 2], unsupervised learning [41, 5], and generative modeling [25, 13, 36].

A CNN consists of multiple spatially compact filters which convolve over an input image, followed typically by normalizations [20], and nonlinearities. The small spatial extent of the convolutional kernel, with its associated weight sharing properties make them efficient and translation equivariant. However, this also implies that the receptive field of the kernel is limited due its small spatial extent. The local nature of the convolution kernels prevents them from capturing the global context of the image. The long-range dependency, i.e., a larger receptive field, is achieved through stacking multiple CNN layers and reducing the spatial dimension by pooling operations. However, it has been observed that the features from this kind of architecture tend to be more receptive towards texture than the shape of the object. For example, [11] tackle this problem by using a better shape-biased dataset like Stylized-ImageNet. As opposed to this, incorporating the shape bias more directly without changing training-sets is a natural choice. As we know, convolutional operations intrinsically represent frequency selective operations while shape is related to geometric concepts rather than specific frequency bands. Therefore, to promote shape-awareness different types of operations, that are more directly shape-sensitive are needed.

In this work, we frame vision tasks like classification, through geometrical properties of the object’s shape. Rigid as well as non-rigid aspects of shape can be described in terms of geometric moments. Geometric moments are a very specific type of weighted averages of image pixel intensities, where the weights are drawn from certain polynomial-type basis function. This operation can be expressed as a projection of the image on the bases. While classic theoretical development around moments used specific choices of the bases functions, their application to difficult tasks like image classification has remained very limited. In this paper, we revisit moments as a learnable spatial operation; where we introduce modules that are motivated by the image-projection analogy, but we leave the bases to be learned end-to-end in a task-specific manner.

Geometric moments have a long history in the vision community for a wide variety of applications ranging from invariant pattern recognition [19], segmentation [30] and 3D shape recognition [40]. We propose a deep-learning based architecture to extract invariant image moments for classification tasks. Our architecture consists of two streams of convolutional networks; one extracts features corresponding to the object, i.e., remove the background from the image, and the second network learns the bases from a 2D coordinate grid. Geometric moments are computed by projecting features of the image to the learned bases. In order to learn task-specific invariant moments to deformations, size, and location, we learn a simple transformation of the coordinate grid and compute the geometric moments at multiple levels. The geometric moment is beneficial in two ways: (1) it captures long-range dependency without using any pooling layer, or reducing the spatial dimension, (2) the spatial transformation of the coordinate grid acts as an attention mechanism. The computation cost of the geometric moment is linear in the spatial dimension.

In particular, the proposed Deep Geometric Moment (DGM) architecture provides four key benefits compared to existing models.

- First, the model generates discriminative features for classification task by accounting for shape information through the proposed deep geometric moments.
- Second, our model outperforms existing ResNet models on standard datasets without using any pooling layer or reducing the spatial dimension.
- Third, it provides an easy access to interpretable features at any level by simple re-projection of moments
- Finally, compared to existing models, the DGM model only requires finetuning of the coordinate basis pipeline without retraining all the model parameters.

Our goal is not to outperform all the latest developments in vision, but to show that our proposed model can perform comparably to standard models when trained from scratch, produces interpretable results, and is easier to finetune for transfer-learning.

2 Geometric moment

A *moment* for a given two-dimensional piece-wise continuous function $f(x, y)$ is defined as:

$$m_{pq} = \int_{-\infty}^{\infty} \int_{-\infty}^{\infty} x^p y^q f(x, y) dx dy, \quad (1)$$

where, (x, y) is the 2D coordinate and $(p + q)$ is the order of the moment. By uniqueness theorem [19], if $f(x, y)$ is piece-wise bounded continuous function (i.e. it is non-zero only on a compact part of the xy plane), then the moment sequence m_{pq} is uniquely defined for all orders $(p + q)$ by $f(x, y)$. Conversely, $f(x, y)$ is uniquely determined by the sequence m_{pq} .

Equivalently, moments can also be seen as a ‘projection’ of the 2D function, on to certain basis functions, of the form $x^p y^q$. Instead of using bases function of type $x^p y^q$, one can instead also use orthogonal functions like Legendre or Zernike polynomials [38] for better reconstruction.

Image moments are well known invariant shape descriptors, with a long history of use in the computer vision literature, to capture geometrical properties of an image. For example, m_{00} (0^{th} order) represents average pixel intensity, m_{10} (1^{st} order) and m_{01} (1^{st} order) represent xy centroid coordinate and the combination of 1^{st} and 2^{nd} order can be used to compute orientation.

For the task of image classification, we need *discriminative moments*, that are also invariant to certain image transformations like rotation, translation, and scale. An early work by Hu [19] introduced a way to find invariant moments for images. The Hu moments consist of seven moments, mostly a

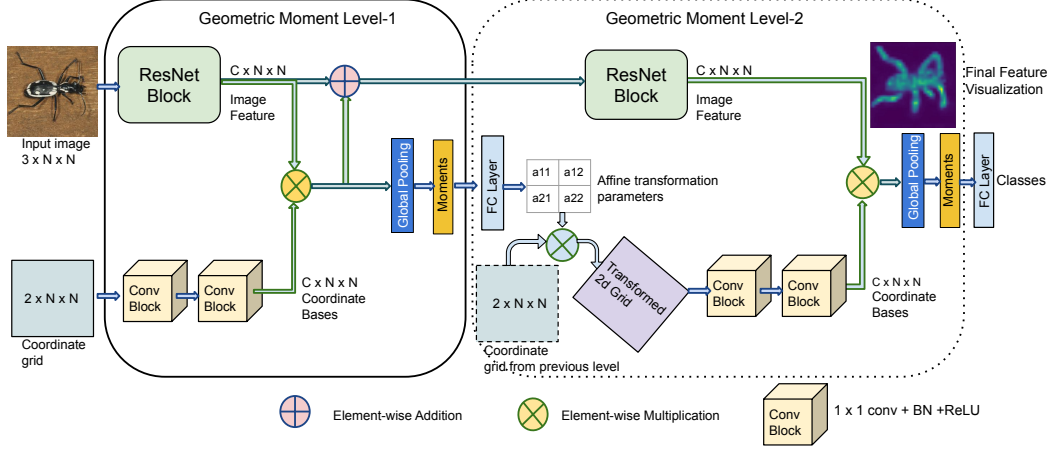


Figure 1: An overview of proposed Deep Geometric Moment (DGM) framework for image classification task. The model consists of two blocks: *Level-1* and *Level-2* that consists of two pipelines : 1) CNN based image feature extraction and 2) coordinate bases computation. The *Level-2* block can be repeated number of times for computing moments, similar to depth concept in deep networks.

combination of lower-order moments invariant under scaling, translation, and rotation. While these basic set of seven Hu moments are provably invariant to rotation, translation, and scale, their use has been limited since their discriminative power is not very high. Developing invariant moments for the Legendre and Zernike polynomials for any arbitrary order is also possible [6, 47, 48, 23, 24, 44], however they also have not shown significant impact on contemporary image classification tasks.

In this paper, we seek to advance a new approach for defining spatial operations for image classification networks, whose structure is motivated by classic moment computation, but whose basis functions are left to be learnt end-to-end by a deep learning network in a task-specific way. This implies that we are not seeking to replicate any of the classical moments in an exact sense, but seek to find ways to fuse moment-like computations and let networks learn the right basis functions for a given task. This approach is described in the next section.

3 Deep geometric moments

CNNs are extremely good at capturing local context and texture information to discriminate images, even in a complex classification task, without an explicit ‘shape’ related operation. On the contrary, geometric moments can capture the shape information exceptionally well and can provide discriminative cues in classifying images, however their discrimination power is quite limited, and generally requires a salient object over a homogeneous background. We advance a new type of architecture that blends the strengths of both approaches. We propose a deep geometric moment model that uses geometric moments along with CNNs for classification by providing access to both shape and texture. The geometric moment for a discrete 2D function is given by the discrete version of (1) :

$$m_{pq} = \sum_x \sum_y x^p y^q I(x, y) \quad (2)$$

In the traditional usage of moments in vision, the number and order of moments is an experimental design choice. Choosing the right number and order of moments is dependent on the underlying tasks; large numbers of moments are useful for image reconstruction, whereas for image classification, higher-order moments are affected by noise, and hence not very useful. Thus, selecting the correct moment orders is important. In our method, we do specify required number of moments (in terms of feature dimension), but the exact basis functions and orders are learnt by the networks end-to-end for specific tasks. Hence we will drop the subscript notation pq and use superscript notation c indicating the feature channel number for moment m .

In our model defined by (3), we use CNNs to extract relevant object features from the given images, and project them onto the learned coordinate bases, *per channel*:

$$m^c = \frac{1}{N \times N} \sum_x \sum_y g^c(x, y) f^c(x, y), \quad (3)$$

where, $N \times N$ is the dimension of the image, $g^c(x, y)$ is a learnable 2D polynomial function, and $f^c(x, y)$ is the image feature at the coordinate location (x, y) , and c refers to the channel dimension of the feature, given by the CNN from the image-feature stream (see top-stream in Figure 1). Next, to account for varying locations, sizes, poses, and deformation; we allow our network to learn affine parameters to deform the 2D coordinate grid appropriately during moment computation.

In summary: the proposed model consists of three components: 1) **Coordinate base computation**: uses a 2D coordinate grid as input and generates the bases, 2) **Image feature computation**: obtains image features through ResNet blocks, and 3) **Affine transform estimation**: to transform the 2D coordinate grid to enable invariance learning. An overview of DGM model is shown in Figure 1. The architecture consist of *Level-1* and *Level-2* blocks, where *Level-1* is fixed, whereas *Level-2* can be replicated multiple times to create deeper networks.

Coordinate base computation: For computing bases, expressed as $g(x, y)$ in (3), a 2D coordinate grid is used as an input. The 2D coordinate grid is represented by $2 \times N \times N$, where $N \times N$ is the dimension of the input image. Each entry in the coordinate grid indicates the normalized 2D pixel locations. $g(x, y)$ in (3) is defined by a neural network that consists of two layers of 1×1 convolution layer followed by a batch-normalization and ReLU layer. This definition of $g(x, y)$ processes each location of the coordinate grid independently. In our experiments, we use only two convolution layers, but one can use more layers to learn more complex or higher-order moments. The output bases are of dimension $C \times N \times N$ where C is the number of moments/channels.

Image feature computation: Referring back to the term $f(x, y)$ in (3), also shown as a ResNet block in Figure 1, takes the image of dimension $3 \times N \times N$ as input, and outputs a feature of dimension $C \times N \times N$. $f(x, y)$ is implemented as a conventional ResNet block [16] with 3×3 filter kernel. Note that the geometric moments are insufficient for capturing local features in the image, whereas the CNNs with a kernel size of 3×3 or greater are very efficient in capturing local properties. Therefore, we use a kernel of size 3×3 in ResNet blocks, which is a common choice in state-of-the-art ResNet-based models. These image features from ResNet block are then projected on the bases by performing element-wise multiplication, and moments are obtained by using global pooling on the projected features. Note that unlike the conventional definition of geometric moment (1) where a same 2D image is projected to each basis, in our method, different feature maps are projected to each basis. Projected feature map on the bases highlights the important region in the feature map and hence can also be used as an attention map.

Affine transformation estimation: We first use the canonical coordinate grid to compute the moments, and predict the affine parameters using these moments. The prediction network consists of two fully-connected layers with a non-linear activation. The prediction network takes the canonical moments ($1 \times C$) as input and outputs the affine parameters ($C \times 6$) for each feature channel. Then, the 2D coordinate grid C_G is transformed according to: $C'_G = \begin{bmatrix} a_{11} & a_{12} \\ a_{21} & a_{22} \end{bmatrix} \times C_G + \begin{bmatrix} t_x \\ t_y \end{bmatrix}$, where, the 2×2 matrix is the predicted affine parameters, t_x and t_y are the predicted translation parameters and C'_G is the transformed 2D coordinate grid. We then use these transformed coordinate grids to generate new bases and compute new moments, for each channel. It is arguable that affine parameters are also limited in providing needed invariance, but this choice is shown as efficient and already leading to good performance.

3.1 DGM classification model

The proposed DGM network as shown in Figure 1 makes uses of computed coordinate bases, convolution network based features, and affine transformation estimation, trainable end-to-end. The functionality of the model comprises of: 1) image feature pipeline that transforms an image to features through ResNet blocks, and 2) geometric moment pipeline that generates the bases, computes the affine parameters and moments. The proposed model does not use any pooling layer or reduces the spatial dimensions across the networks. This preserves the shape of the object, as opposed to

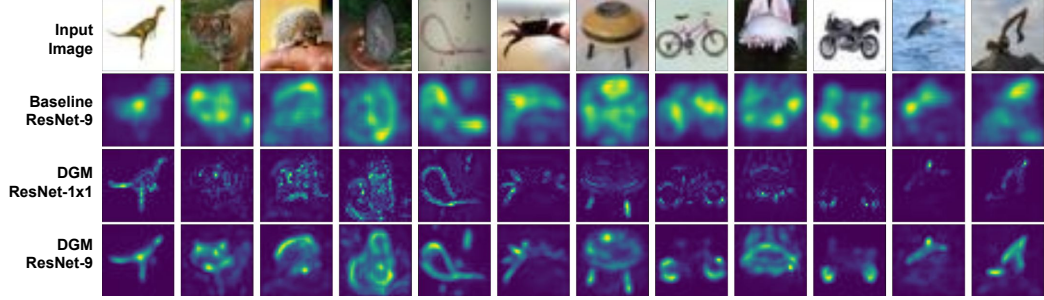


Figure 2: *Level-4* feature visualization from different models on the CIFAR-100 datasets. The DGM model captures better object shape compared to the baseline model.

pooling or reducing the spatial dimension that distorts the final reconstructed shape, limiting its interpretability. We also use the same number of feature channels in each ResNet layers for simplicity.

As shown in Figure 1, *Level-1*, uses the canonical coordinate grid to generate the bases, and the ResNet block to generate feature from the image. We then project this feature on the bases to compute the moments. The projected feature acts as an attention map, and is added back to the original feature. This feature map and geometric moments are then passed to *Level-2*.

The *Level-2* contains a ResNet block to further process the features. This level also predicts the affine parameters based on the moments from the previous level and transforms the coordinate grid to regenerate the bases. Figure 1 shows only two levels, but one can repeat the *Level-2* block multiple times for added depth. The moments from the final level are used as an input to fully-connected layer to generate class probabilities for the classification task.

Feature Visualization: To visualize the shape-awareness brought by the DGM approach, we describe a particular to visualize the learnt features, that also highlight the object shape. By the uniqueness theorem [19], moments can be used to reconstruct the original input, provided the bases are complete. In our case, our learnt bases are under-complete. Using the moments as combination weights on the projected features given by:

$$V = \sum_c m^c (G^c \otimes F^c), \quad (4)$$

where, m^c is the moment, G^c is the basis and F^c is the image feature for channel c , and \otimes is element-wise multiplication, we get a visualization of shape-related information in the features.

4 Experimental results

We evaluate the proposed method for image classification on standard datasets: CIFAR-10, CIFAR-100 [26], and ILSVRC-2012 ImageNet [33] to validate the effectiveness of our model. The performance of our model is compared to the baseline model and standard ResNet models [16], across classification accuracy (in %), number of parameters (in Million M), and number of floating-point operations (flops in Giga G). The baseline ResNet model is constructed in the same manner as our DGM model but without projection onto the coordinate bases. The baseline models are similar to standard ResNet models without pooling layers or reducing the spatial dimension. Along with the classification performance, we also compare the feature reconstruction qualitatively. The visualization for the baseline is just a weighted sum of the final Conv layer activation based on the global feature.

4.1 Experiments on CIFAR dataset

For CIFAR experiments, we choose both the coordinate grid dimension and image feature spatial dimension as 32×32 . The number of coordinate bases and image feature channels is 256 across each level, for all the experiments. However, one can also use different number of channels, i.e., fewer filters on the top, and several more filters at the bottom, similar to a standard ResNet model. *Additional training details are provided in the appendix.* Next, we present experiments and discuss the reasoning behind certain choices of hyperparameters in our model and comparison with the baseline and standard ResNet model.

Table 1: Performance comparison of DGM model with increasing levels on CIFAR datasets

Model	Params (M)	CIFAR 10 (%)	CIFAR 100 (%)
DGM Level-1	0.44	84.79	59.07
DGM Level-2	1.37	88.77	68.07
DGM Level-3	2.30	90.09	69.72
DGM Level-4	3.23	90.28	70.56
DGM Level-4 w/o affine	2.03	88.47	66.6

Table 2: Performance comparison of DGM and baseline ResNet models on CIFAR datasets

Model	Params (M)	CIFAR 10 (%)	CIFAR 100 (%)
Baseline- 1×1	1.67	88.51	66.82
DGM- 1×1	3.23	90.28	70.56
Baseline ResNet-9	4.90	93.68	76.28
DGM ResNet-9	6.49	94.52	77.56

How many levels do we need? In this experiment the ResNet block in the image feature pipeline consists of only 1×1 filter kernels, except the first Conv layer. There is no interaction between neighboring pixels in this setting, and the only interaction is through geometric moments and affine transformation of the coordinate grid. Each level in our DGM model consists of a ResNet block with two ResNet layers, a coordinate bases generator defined with two convolutional layers, and two fully connected layers for affine parameters prediction. This setting helps us understand the overall contribution made by the coordinate bases and the affine transformation.

Table 1 reports DGM model’s classification performance as well as number of parameters as we increase the number of levels in the model. In *Level-1*, we simply use the canonical coordinate grid to generate the bases. The results show that DGM *Level-2* performs significantly better than DGM *Level-1* on both the CIFAR-10 and CIFAR-100 datasets. This performance improvement reflects the effectiveness of transforming the coordinate grid to regenerate better bases. We also see that the performance difference between the *Level-3* and *Level-4* models is minimal. In DGM *Level-4* w/o affine transform we do not transform the coordinate grid, hence the bases in this case remain same for every images. We can see without affine transformation the performance of the model drops indicating the effectiveness of using affine transformation. Also, increasing the levels beyond 4 does not significantly improve the classification performance, but is accompanied by a large increase in the number of parameters and computation; hence, we use only *Level-4* in all the experiments.

Comparison with baseline ResNet model: We use global pooling on the features from the last ResNet layer of the baseline model to get the final feature vector for classification. In Table 2, the baseline- 1×1 is the ResNet model with 1×1 filter kernel in every ResNet layer. The baseline ResNet-9 model is based on the standard ResNet-9 model with a constant number of feature channels (256) in every layer, without reducing the spatial dimensions. DGM- 1×1 is the proposed model with 4 levels and 1×1 convolutional kernel in the ResNet Blocks. DGM ResNet-9 is also of 4 levels with ResNet-9 as the image feature pipeline.

Table 2 shows that the proposed DGM models perform better than the baselines on both CIFAR datasets. The improvement in performance validates the effectiveness of the proposed model. We also observe that when the number of parameters in the model is lower (baseline- 1×1), we get a higher performance gain with the DGM.

Comparison with standard ResNet model: Table 3 compares the proposed DGM model with conventional ResNet models [16]. In the standard ResNet model, the number of feature channels in each ResNet block is (64, 128, 256, 512), whereas, in our DGM model, the number of feature channels is 256 across all levels. The naming of our DGM model is based on the number of convolution layers used in the image feature pipeline. Table 3 shows that the proposed DGM models perform better than the standard ResNet models on both CIFAR-10 and CIFAR-100 datasets; interestingly, the accuracy of DGM ResNet-18 is better than the standard ResNet-50 model. However, the computation cost (in terms of flops) in our DGM model is much higher than conventional ResNet. This higher cost is attributable to the fact that we do not reduce the spatial dimension of the image features. However, one can reduce the computation cost in image pipeline by using some of the tricks in [18] and [34]. In Table 3, DGM ResNet-66* has channel-wise convolutions, which reduces the number of parameters and computation, but performs comparable to DGM model with conventional ResNet layers.

Feature visualization: The final feature vectors can be easily visualized by a reconstruction step as given by (4). It highlights the relevant regions of the image that contribute to final decision. Figure 2 shows *Level-4* feature visualization as a heatmap for few randomly selected images from CIFAR-100

Table 3: Performance improvements of DGM models over standard ResNet model on CIFAR datasets

Model	Params (M)	Flops (G)	CIFAR-10 (%)	CIFAR-100 (%)
ResNet-18	11.17	0.57	95.37	77.35
DGM ResNet-18	11.61	10.24	95.51	80.60
ResNet-50	23.52	1.30	95.47	80.10
DGM ResNet-34	21.06	19.91	96.27	82.13
DGM ResNet-66*	4.50	2.95	96.33	82.19

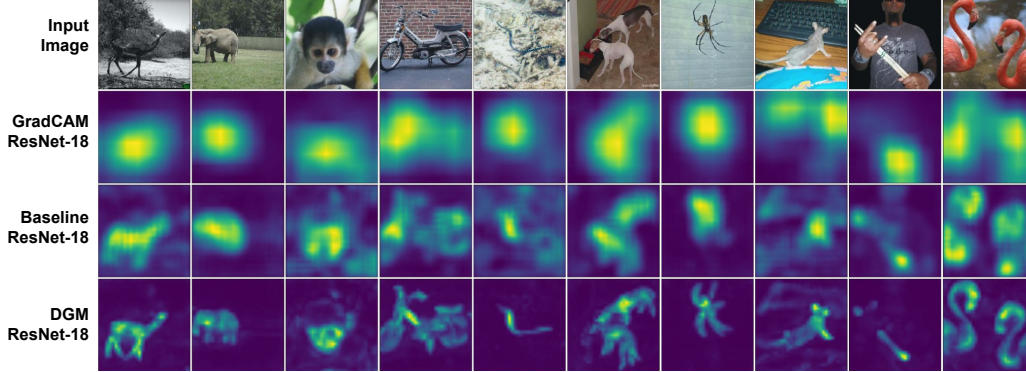


Figure 3: Feature visualization of different models on ImageNet. For the standard ResNet model we use GradCAM for the visualization. Note that our DGM model produces very sharp object shape.

dataset for our DGM models and baseline ResNet-9 model. The heatmap from the baseline is diffuse, making it hard to glean detailed object shape, whereas the heatmap from the DGM models capture the shape much more clearly while also improving the classification accuracy.

Figure 2 compares visualization from DGM ResNet-1 \times 1 and DGM ResNet-9 models. In DGM ResNet-1 \times 1 model, the heatmap is sparser compared to DGM ResNet-9. This sparsity shows inefficiency of geometric moments in capturing local image features when compared to the CNN models with kernel size 3 \times 3 or larger.

Table 4: Performance comparison of DGM model with standard ResNet model on ImageNet dataset

Model	Params (M)	Flops (G)	Accuracy (%)
Baseline ResNet-18	9.89	9.86	68.42
ResNet-18	11.69	1.82	71.23
DGM ResNet-18	11.88	10.27	72.36
ResNet-34	21.80	3.68	74.58
DGM ResNet-34	21.32	19.94	75.63
ResNet-50	25.56	4.12	76.92
DGM ResNet-50	23.51	17.59	77.06
DGM ResNet-66*	4.76	2.99	72.69

4.2 Experiments on ImageNet dataset

The standard ResNet model uses an image size of 224 \times 224 as input. Using this resolution with our model is computationally expensive, since we do not down-sample the spatial dimension of the image features. Therefore, we divide the 256 \times 256 image into 8 \times 8 patches, and use a linear embedding layer similar to [9] to reduce the spatial dimension to 32 \times 32, followed by the DGM model. For the embedding layer, we use a convolution layer with 8 \times 8 kernel and stride of 8. *Training details for the same are provided in appendix*

Table 4 compares the performance of DGM model with baseline and standard ResNet models. The results show that our DGM model is better than the baseline and standard ResNet model while using the similar number of parameters. We also observe that DGM model’s computation cost (in terms of flops) is much higher than the standard ResNet models, but can be reduced by using channel-wise

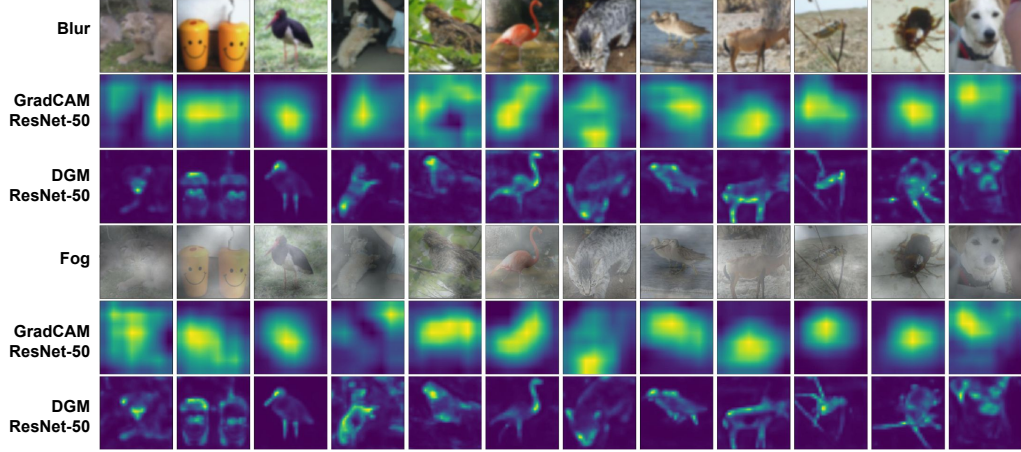


Figure 4: Visualization from DGM and standard ResNet model under two different color distortion (Blur (1st row) and Fog (4th row) from Imagenet-C). Our model (3rd and 6th row), is able to produce consistent shape across different distortion compared to standard ResNet (2nd and 5th row).

Table 5: Classification performance on fine-tuning of pre-trained ImageNet DGM model on CIFAR datasets

Model	Params (M)	CIFAR 10(%)	CIFAR 100(%)
DGM ResNet-18	11.69	93.79	75.83
DGM ResNet-34	21.32	94.01	77.51
DGM ResNet-66*	4.76	93.87	75.92

Table 6: Mean Corruption Error (mCE) comparison of DGM with standard ResNet model on ImageNet-c dataset

Model	Params (M)	Clean ↑ Acc. (%)	mCE ↓ (%)
ResNet-50	25.56	76.92	74.97
DGM ResNet-50	23.51	77.06	71.74

convolutions similar to MobileNet [18], in the image feature pipeline. The DGM ResNet-66* is based on MobileNet, and performs comparable to the standard ResNet with similar computation cost.

Further, we show that DGM model eases visualization and interpretability of feature maps as compared to the GradCAM [35] visualizations. As shown in Fig3, the GradCAM visualizations of standard ResNet-18 model generates a blob-like shape around the critical region in the image, with no discernible object shape. We see that while it gets better for baseline ResNet-18 model, the heatmaps are still diffuse, and the shapes are not very distinct. However, with the DGM model, the object shapes are evidently crisp, with improved classification accuracies as well. *Additional qualitative results for analysis are provided in the Appendix.*

DGM finetuning: For DGM finetuning, we only need to retrain the coordinate bases pipeline, and the final classifier layer, while freezing the image feature exaction pipeline. The coordinate bases pipeline contains significantly fewer parameters and requires less computation. We finetune our ImageNet pre-trained DGM model for only 30 epochs on CIFAR-10 and CIFAR-100 datasets. The network is finetuned using a SGD optimizer with cosine decay learning rate and an initial learning rate of 0.01. Table 5 shows the accuracy of the finetuned model on the CIFAR-10 and CIFAR-100 datasets. The performance of the finetuned model drops as compared to DGM trained from scratch, but it performs equally well to the standard ResNet model trained from scratch on these datasets.

Performance under color distortion: We evaluate the effect of color distortions on DGM performance by testing it on ImageNet-C [17]. The ImageNet pretrained DGM model used for this experiment does not use any color augmentation during training, making it a sufficiently challenging task. The DGM ResNet-50 and GradCAM ResNet-50 visualization for two distortions are shown in Figure 4. The figure shows that our model captures the object shape very well under different challenging distortions like fog and blur. The GradCAM heatmap for the ResNet-50 is not very consistent across distortions as compared to our DGM model. For quantitative performance we use mean Corruption Error (mCE) metric (lower is better) [17]. We choose our DGM model such that it performs comparably to the standard ResNet-50 model on clean images, but with fewer parameters. Table 6 shows DGM model provides an improvement of **3.2 %** on the corrupted images.

Table 7: Semantic segmentation performance on PASCAL VOC 2012 [10] and Cityscapes [7] val set in terms of mean intersection over union (mIoU)

Backbone Segmentation head	ResNet-50 DeepLabv3Plus	DGM-ResNet-50 1×1 Conv	DGM-ResNet-50 DeepLabv3Plus
PASCAL VOC (mIoU)	78.36	78.43	79.89
Cityscapes (mIoU)	75.34	74.77	76.03

4.3 Semantic image segmentation

The DGM model is evaluated on the PASCAL VOC 2012 [10] and Cityscapes [7] semantic segmentation benchmark datasets. We use a *Level-5* DGM model with ResNet-50 as the image-feature pipeline pretrained on the ImageNet dataset. The number of parameters in the *Level-5* DGM ResNet-50 is almost the same as the standard ResNet-50 model (~ 25 M). We use the same training hyperparameters as in DeepLabv3+ model [4]. We test the effectiveness of our model with two different segmentation heads; first, with just two 1×1 Conv layers as segmentation head that takes the final 2D features rescaled by factor of 4, and second, DeepLabv3+ segmentation head which consists of astrous convolution with different rates to capture long range dependencies. In Table 7 we observe that even with a very simple segmentation head our model performs similar to the standard DeepLabv3+ model on both datasets. This shows that geometric moments are effective in capturing long range dependencies. Our model shows improvements of 1.5% points on Pascal Voc and 0.7% points on Cityscapes val sets compared to the standard ResNet model.

5 Related work

Geometric moments and deep networks: There has been prior work in integrating geometric moments with deep networks, as specifically applied to 3D shape classification, from point-cloud data. For example, geodesic moment-based features from an auto-encoder were used to classify 3D shapes [29]. On the other hand, CNNs were used as a polynomial function to learn bases, and the needed affine transformation parameters for 3D point cloud data based shape classification [22]. This line of work was extended in [28] which uses graph CNN to capture local features of the 3D object. More recently, [39] and [45] replaced the conventional global average pooling in CNN models with invariant Zernike moment-based pooling for image classification task. Contrary to these methods, our approach learns bases as well as the affine parameters. Note that our work is different from these approaches because a) we are interested in natural image classification where moment computation is challenging compared to 3D shape classification, due to intensity variation, background variation, occlusions, etc, b) architecturally our approach is more involved compared to processing 3D object that are specified directly in terms of coordinate locations.

Vision transformers: In recent years, self attention based transformer models [42] have gained prominence for various vision tasks [9, 46, 49, 14]. The vision transformer (ViT) model achieves long-range dependency through an attention mechanism that computes the similarity between features over the entire spatial dimension. ViT provides interpretability through the attention map, but they are difficult to train from scratch and forward computation scales quadratically in image size.

Spatial transformer network (STN) [21] predicts the affine transformation parameters for classifying images that help in maximizing object detection accuracy, and transforms the 2D CNN feature grid accordingly. The spatial transformation of the feature grid acts as an attention module and brings invariance to rotation, translation, scale, and different warping of the image data. [8] presents a spatially deformable convolution and pooling kernel to bring invariance under spatial transform. In our work, we do not transform the CNN feature grid and instead a *2D* coordinate grid that is much simpler in terms of computation and implementation.

Feature visualization: Most general CNNs have a very low feature resolution/dimension in the final layers, which makes it really difficult to visualize them. Most methods use gradient propagation [35, 1] or optimization based visualization [43] to tackle this limitation. Our visualization method is quite direct, and in our opinion, the most straightforward approach for our case, and doesn't require solving any optimization problem or gradient propagation.

6 Conclusion

In this work we propose a geometric moment-based deep learning model that explicitly captures the shape-related information in a end-to-end learnable fashion. The DGM model is shown to improve interpretability of features, while also learning discriminative features. The quantitative and qualitative results on standard datasets on image classification as well as segmentation show that our method performs better than the corresponding baseline and standard ResNet models. In addition, DGM model provides easy interpretability at different levels in the network while also providing ease of finetuning on a given dataset. Further, our model captures the object’s shape even under extreme affine and color aberrations, while also performing better than existing approaches. We believe that DGM has the potential to improve the performance of other vision tasks such as object detection and generation and can be generalized to other modalities like video, RGBD, and volumetric data.

References

- [1] L. Chen, J. Chen, H. Hajimirsadeghi, and G. Mori. Adapting grad-cam for embedding networks. In *Proceedings of the IEEE/CVF Winter Conference on Applications of Computer Vision*, pages 2794–2803, 2020.
- [2] L.-C. Chen, M. D. Collins, Y. Zhu, G. Papandreou, B. Zoph, F. Schroff, H. Adam, and J. Shlens. Searching for efficient multi-scale architectures for dense image prediction. *arXiv preprint arXiv:1809.04184*, 2018.
- [3] L.-C. Chen, G. Papandreou, I. Kokkinos, K. Murphy, and A. L. Yuille. Deeplab: Semantic image segmentation with deep convolutional nets, atrous convolution, and fully connected crfs. *IEEE transactions on pattern analysis and machine intelligence*, 40(4):834–848, 2017.
- [4] L.-C. Chen, Y. Zhu, G. Papandreou, F. Schroff, and H. Adam. Encoder-decoder with atrous separable convolution for semantic image segmentation. In *Proceedings of the European conference on computer vision (ECCV)*, pages 801–818, 2018.
- [5] X. Chen, Y. Duan, R. Houthoofd, J. Schulman, I. Sutskever, and P. Abbeel. Infogan: Interpretable representation learning by information maximizing generative adversarial nets. In *Proceedings of the 30th International Conference on Neural Information Processing Systems*, pages 2180–2188, 2016.
- [6] C.-W. Chong, P. Raveendran, and R. Mukundan. Translation and scale invariants of legendre moments. *Pattern recognition*, 37(1):119–129, 2004.
- [7] M. Cordts, M. Omran, S. Ramos, T. Rehfeld, M. Enzweiler, R. Benenson, U. Franke, S. Roth, and B. Schiele. The cityscapes dataset for semantic urban scene understanding. In *Proceedings of the IEEE conference on computer vision and pattern recognition*, pages 3213–3223, 2016.
- [8] J. Dai, H. Qi, Y. Xiong, Y. Li, G. Zhang, H. Hu, and Y. Wei. Deformable convolutional networks. In *Proceedings of the IEEE international conference on computer vision*, pages 764–773, 2017.
- [9] A. Dosovitskiy, L. Beyer, A. Kolesnikov, D. Weissenborn, X. Zhai, T. Unterthiner, M. Dehghani, M. Minderer, G. Heigold, S. Gelly, et al. An image is worth 16x16 words: Transformers for image recognition at scale. *arXiv preprint arXiv:2010.11929*, 2020.
- [10] M. Everingham, S. Eslami, L. Van Gool, C. K. Williams, J. Winn, and A. Zisserman. The pascal visual object classes challenge: A retrospective. *International journal of computer vision*, 111(1):98–136, 2015.
- [11] R. Geirhos, P. Rubisch, C. Michaelis, M. Bethge, F. A. Wichmann, and W. Brendel. Imagenet-trained cnns are biased towards texture; increasing shape bias improves accuracy and robustness. *arXiv preprint arXiv:1811.12231*, 2018.
- [12] R. Girshick, J. Donahue, T. Darrell, and J. Malik. Rich feature hierarchies for accurate object detection and semantic segmentation. In *Proceedings of the IEEE conference on computer vision and pattern recognition*, pages 580–587, 2014.
- [13] I. Goodfellow, J. Pouget-Abadie, M. Mirza, B. Xu, D. Warde-Farley, S. Ozair, A. Courville, and Y. Bengio. Generative adversarial nets. *Advances in neural information processing systems*, 27, 2014.
- [14] M.-H. Guo, J.-X. Cai, Z.-N. Liu, T.-J. Mu, R. R. Martin, and S.-M. Hu. Pct: Point cloud transformer. *Computational Visual Media*, 7(2):187–199, 2021.

- [15] K. He, G. Gkioxari, P. Dollár, and R. Girshick. Mask r-cnn. In *Proceedings of the IEEE international conference on computer vision*, pages 2961–2969, 2017.
- [16] K. He, X. Zhang, S. Ren, and J. Sun. Deep residual learning for image recognition. In *Proceedings of the IEEE conference on computer vision and pattern recognition*, pages 770–778, 2016.
- [17] D. Hendrycks and T. Dietterich. Benchmarking neural network robustness to common corruptions and perturbations. *arXiv preprint arXiv:1903.12261*, 2019.
- [18] A. G. Howard, M. Zhu, B. Chen, D. Kalenichenko, W. Wang, T. Weyand, M. Andreetto, and H. Adam. Mobilenets: Efficient convolutional neural networks for mobile vision applications. *arXiv preprint arXiv:1704.04861*, 2017.
- [19] M.-K. Hu. Visual pattern recognition by moment invariants. *IRE transactions on information theory*, 8(2):179–187, 1962.
- [20] S. Ioffe and C. Szegedy. Batch normalization: Accelerating deep network training by reducing internal covariate shift. In *International conference on machine learning*, pages 448–456. PMLR, 2015.
- [21] M. Jaderberg, K. Simonyan, A. Zisserman, et al. Spatial transformer networks. *Advances in neural information processing systems*, 28:2017–2025, 2015.
- [22] M. Joseph-Rivlin, A. Zvirin, and R. Kimmel. Momen (e) t: Flavor the moments in learning to classify shapes. In *Proceedings of the IEEE/CVF International Conference on Computer Vision Workshops*, pages 0–0, 2019.
- [23] A. Khotanzad and Y. H. Hong. Invariant image recognition by zernike moments. *IEEE Transactions on pattern analysis and machine intelligence*, 12(5):489–497, 1990.
- [24] H. S. Kim and H.-K. Lee. Invariant image watermark using zernike moments. *IEEE transactions on Circuits and Systems for Video Technology*, 13(8):766–775, 2003.
- [25] D. P. Kingma and M. Welling. Stochastic gradient vb and the variational auto-encoder. In *Second International Conference on Learning Representations, ICLR*, volume 19, page 121, 2014.
- [26] A. Krizhevsky, G. Hinton, et al. Learning multiple layers of features from tiny images. *Citeseer*, 2009.
- [27] A. Krizhevsky, I. Sutskever, and G. E. Hinton. Imagenet classification with deep convolutional neural networks. *Advances in neural information processing systems*, 25:1097–1105, 2012.
- [28] D. Li, X. Shen, Y. Yu, H. Guan, H. Wang, and D. Li. Ggm-net: Graph geometric moments convolution neural network for point cloud shape classification. *IEEE Access*, 8:124989–124998, 2020.
- [29] L. Luciano and A. B. Hamza. Deep learning with geodesic moments for 3d shape classification. *Pattern Recognition Letters*, 105:182–190, 2018.
- [30] A. P. Reeves, R. J. Prokop, S. E. Andrews, and F. P. Kuhl. Three-dimensional shape analysis using moments and fourier descriptors. *IEEE Transactions on Pattern Analysis and Machine Intelligence*, 10(6):937–943, 1988.
- [31] S. Ren, K. He, R. Girshick, and J. Sun. Faster r-cnn: Towards real-time object detection with region proposal networks. *Advances in neural information processing systems*, 28:91–99, 2015.
- [32] O. Ronneberger, P. Fischer, and T. Brox. U-net: Convolutional networks for biomedical image segmentation. In *International Conference on Medical image computing and computer-assisted intervention*, pages 234–241. Springer, 2015.
- [33] O. Russakovsky, J. Deng, H. Su, J. Krause, S. Satheesh, S. Ma, Z. Huang, A. Karpathy, A. Khosla, M. Bernstein, et al. Imagenet large scale visual recognition challenge. *International journal of computer vision*, 115(3):211–252, 2015.
- [34] M. Sandler, A. Howard, M. Zhu, A. Zhmoginov, and L.-C. Chen. Mobilenetv2: Inverted residuals and linear bottlenecks. In *Proceedings of the IEEE conference on computer vision and pattern recognition*, pages 4510–4520, 2018.
- [35] R. R. Selvaraju, M. Cogswell, A. Das, R. Vedantam, D. Parikh, and D. Batra. Grad-cam: Visual explanations from deep networks via gradient-based localization. In *Proceedings of the IEEE international conference on computer vision*, pages 618–626, 2017.

- [36] R. Singh, P. Turaga, S. Jayasuriya, R. Garg, and M. Braun. Non-parametric priors for generative adversarial networks. In *International Conference on Machine Learning*, pages 5838–5847. PMLR, 2019.
- [37] C. Szegedy, W. Liu, Y. Jia, P. Sermanet, S. Reed, D. Anguelov, D. Erhan, V. Vanhoucke, and A. Rabinovich. Going deeper with convolutions. In *Proceedings of the IEEE conference on computer vision and pattern recognition*, pages 1–9, 2015.
- [38] M. R. Teague. Image analysis via the general theory of moments. *Josa*, 70(8):920–930, 1980.
- [39] T. Theodoridis, K. Loumponias, N. Vretos, and P. Daras. Zernike pooling: Generalizing average pooling using zernike moments. *IEEE Access*, 9:121128–121136, 2021.
- [40] M. Tuceryan. Moment-based texture segmentation. *Pattern recognition letters*, 15(7):659–668, 1994.
- [41] W. Van Gansbeke, S. Vandenhende, S. Georgoulis, M. Proesmans, and L. Van Gool. Scan: Learning to classify images without labels. In *European Conference on Computer Vision*, pages 268–285. Springer, 2020.
- [42] A. Vaswani, N. Shazeer, N. Parmar, J. Uszkoreit, L. Jones, A. N. Gomez, L. Kaiser, and I. Polosukhin. Attention is all you need. In *Advances in neural information processing systems*, pages 5998–6008, 2017.
- [43] J. Wagner, J. M. Kohler, T. Gindele, L. Hetzel, J. T. Wiedemer, and S. Behnke. Interpretable and fine-grained visual explanations for convolutional neural networks. In *Proceedings of the IEEE/CVF Conference on Computer Vision and Pattern Recognition*, pages 9097–9107, 2019.
- [44] L. Wang and G. Healey. Using zernike moments for the illumination and geometry invariant classification of multispectral texture. *IEEE Transactions on Image Processing*, 7(2):196–203, 1998.
- [45] J. Wu, S. Qiu, Y. Kong, Y. Chen, L. Senhadji, and H. Shu. Momentsnet: a simple learning-free method for binary image recognition. In *2017 IEEE International Conference on Image Processing (ICIP)*, pages 2667–2671. IEEE, 2017.
- [46] L. Yuan, Y. Chen, T. Wang, W. Yu, Y. Shi, Z. Jiang, F. E. Tay, J. Feng, and S. Yan. Tokens-to-token vit: Training vision transformers from scratch on imagenet. *arXiv preprint arXiv:2101.11986*, 2021.
- [47] H. Zhang, H. Shu, G. Coatrieux, J. Zhu, Q. J. Wu, Y. Zhang, H. Zhu, and L. Luo. Affine legendre moment invariants for image watermarking robust to geometric distortions. *IEEE Transactions on Image Processing*, 20(8):2189–2199, 2011.
- [48] H. Zhang, H. Shu, G. N. Han, G. Coatrieux, L. Luo, and J. L. Coatrieux. Blurred image recognition by legendre moment invariants. *IEEE Transactions on Image Processing*, 19(3):596–611, 2009.
- [49] S. Zheng, J. Lu, H. Zhao, X. Zhu, Z. Luo, Y. Wang, Y. Fu, J. Feng, T. Xiang, P. H. Torr, et al. Rethinking semantic segmentation from a sequence-to-sequence perspective with transformers. In *Proceedings of the IEEE/CVF Conference on Computer Vision and Pattern Recognition*, pages 6881–6890, 2021.

A Appendix

This section provides the training details used in the experiments for different datasets and presents additional quantitative and qualitative results for our proposed Deep Geometric Moment (DGM) model.

A.1 Semantic image segmentation

Training details: For PASCAL VOC dataset, we train our model with input size of 512×512 and batch size of 48, and for Cityscapes dataset we train with 768×768 images and batch size of 32. We train models on both datasets with initial learning rate of 0.01 and ‘poly’ learning rate policy (the learning rate is multiplied by $(1 - \frac{iter}{max_iter})^{power}$, where $power = 0.9$). All models are trained with SGD optimizer ($weight_decay = 1e^{-4}$ and $momentum = 0.9$), cross entropy loss and up to 30K iterations.

Qualitative results on Cityscapes: Figure 5 shows qualitative results on the Cityscapes dataset. We observe that the segmentation map from our DGM model is better than the standard ResNet model.

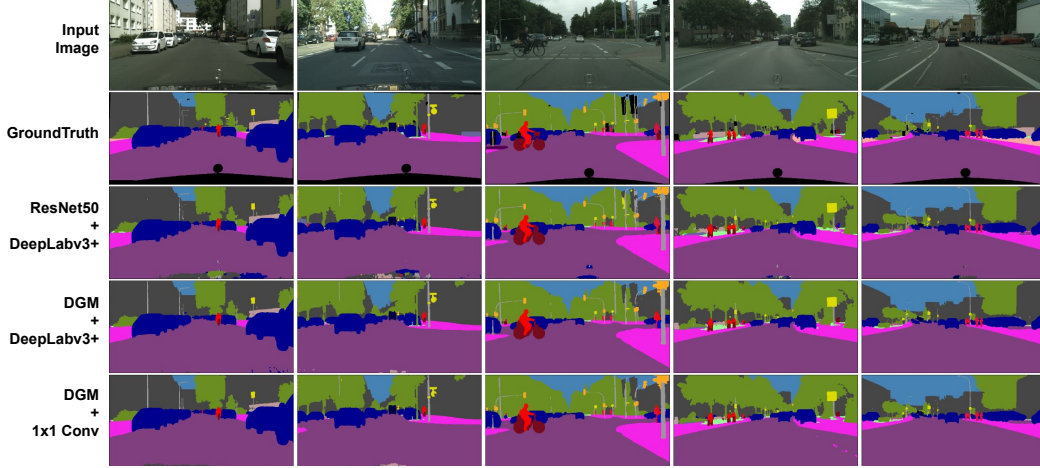


Figure 5: Cityscape segmentation results. The segmentation results from our DGM ResNet-50 model is qualitatively better than the standard ResNet-50 model.

A.2 Training details for image classification

CIFAR: All the models on these datasets are trained up to 150 epochs with a batch size of 128, and SGD optimizer with $momentum = 0.9$ and $weight_decay = 5e^{-4}$. We use cosine learning rate decay with an initial learning rate of 0.1. During training, we augment the dataset with color and affine transformations.

ImageNet: We train all our models on this dataset with a batch size of 256 and up to 100 epoch, and SGD optimizer with $momentum = 0.9$ and $weight_decay = 1e^{-4}$. We use cosine learning rate decay with an initial learning rate of 0.1.

A.3 Performance under affine distortions

Table 8 compares the classification performance of different models under various affine distortions on CIFAR-100 dataset. In this experiment, the images are altered with rotation (R), uniformly selected between $\pm 90^\circ$ and rotation scale and translation (RST), uniformly chosen from $(\pm 90^\circ)$, scale between $[0.7 \text{ and } 1.2]$ and translation between $(\pm 20\%, \text{ in both x and y directions})$.

Table 8: Performance comparison on distorted CIFAR-100 dataset. R stands for rotation and RST stands for rotate, scale and translate

Model	Params(M)	R (%)	RST (%)
Baseline ResNet-18	9.62	72.46	69.62
ResNet-18	11.17	72.65	69.79
DGM ResNet-18	11.62	73.45	71.81
ResNet-50	23.52	74.88	72.43
DGM ResNet-34	21.06	74.91	73.20

Table 8 shows that our DGM model outperforms the baseline as well as the standard ResNet model with a similar number of parameters on both (R) and (RST) distortions. While (RST) distortion is significantly more complex than (R), the performance gain of DGM over the standard ResNet model for (RST) is higher than the (R) distortion. Figure 6 shows that our model has invariance to affine transformations and captures the object shape perfectly well while also outperforming existing classification models under such drastic distortions.

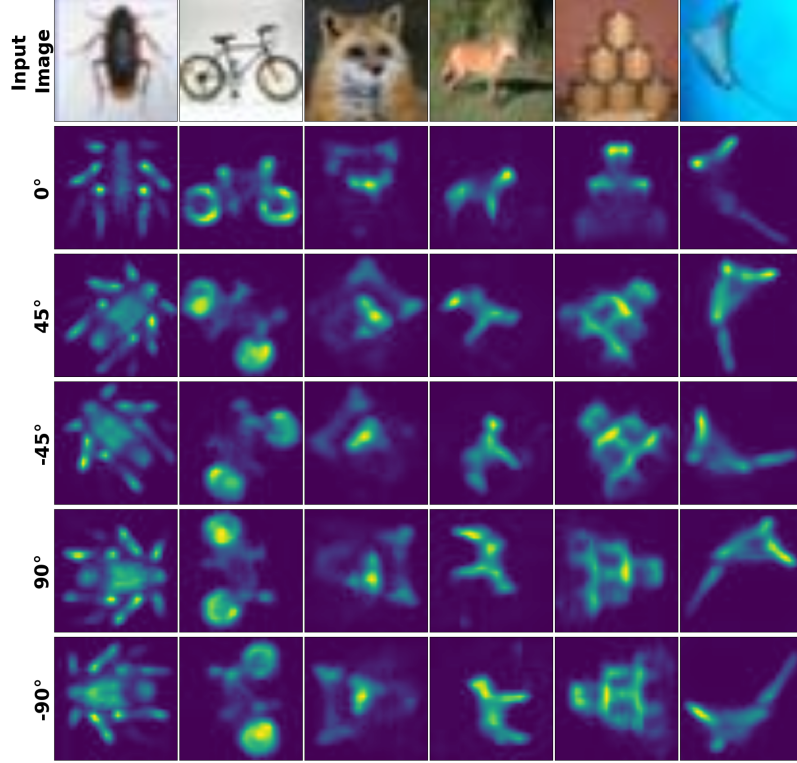


Figure 6: *Level-4* feature visualization from DGM model under different image rotations on CIFAR-100 dataset. The object shape is very well captured across different rotations of the image

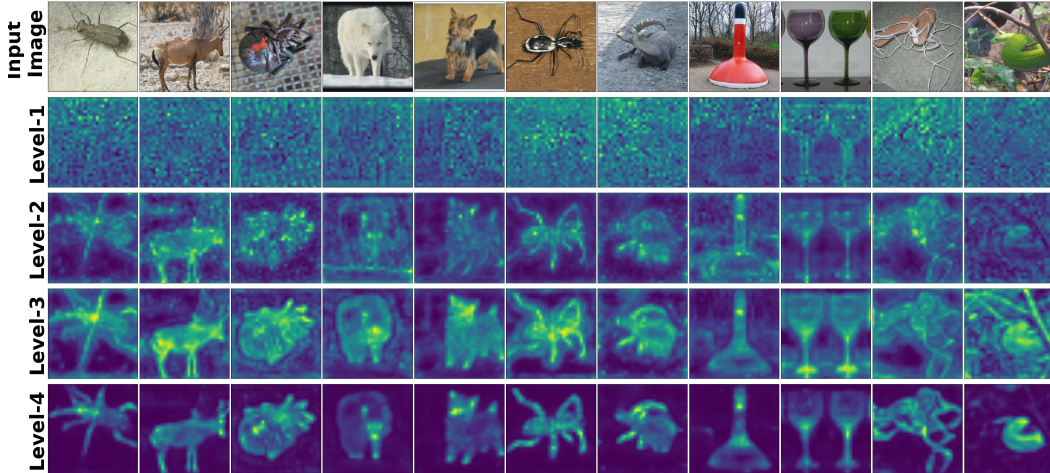


Figure 7: Visualization at different levels for DGM ResNet-34 model on the ImageNet dataset. We note that at higher levels our model is able to separate the background information from the object's shape compared to initial levels.

A.4 All level feature visualization

Figure 7 shows feature visualization at different levels for our DGM model on ImageNet dataset. We observe that in initial levels (*Level-1*, *Level-2*), the visualization is very noisy, but at higher levels, it can separate foreground and background. In the last level (*Level-4*), it is only focusing on the object for the classification.

A.5 Feature visualization across different DGM models

Figure 8 shows *level-4* feature visualization of different DGM models on the ImageNet dataset. All our DGM model produces very clear object shape visualization. We also observe that the objects' shapes for DGM ResNet-34 and DGM ResNet-66* are slightly sharper in some cases compared to DGM-ResNet-18, which is also reflected in the classification accuracy performance.



Figure 8: *Level-4* feature visualization of different DGM models on the ImageNet dataset. Note that all our DGM models produce very sharp object shape. We also observe that the objects' shape for DGM ResNet-34 and DGM ResNet-66* are slightly sharper in some cases compared to DGM-ResNet-18 which is also reflected in the classification accuracy performance.

A.6 Bases visualization

We also observe that bases from *Level-4* of our DGM model, as shown in Figure 9 for two input images, are also indicative of the object shape. The figure compares the same set of bases sampled from 256 bases for the two images. We observe that the final bases are generated based on the input images, so each image gets a unique set of bases.

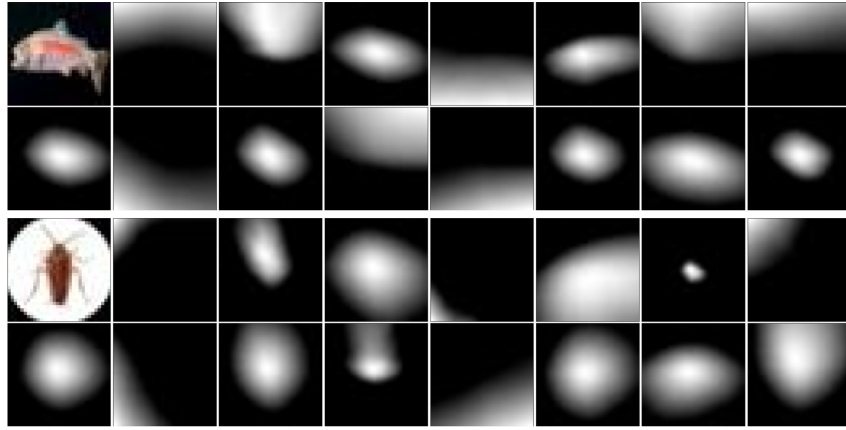


Figure 9: Comparison of bases generated from *Level-4* of our DGM model for two images from CIFAR-100 dataset (top left). Note that the bases from *Level-4* are dependent on the input image.

A.7 Additional visualizations

In this section we provides additional visualizations. Figure 10 shows *Level-4* visualization under different color distortions on ImageNet-C dataset. Figure 11 shows *Level-4* visualization under different rotations on ImageNet dataset. Figure 12 provides additional *Level-4* visualization on ImageNet dataset.

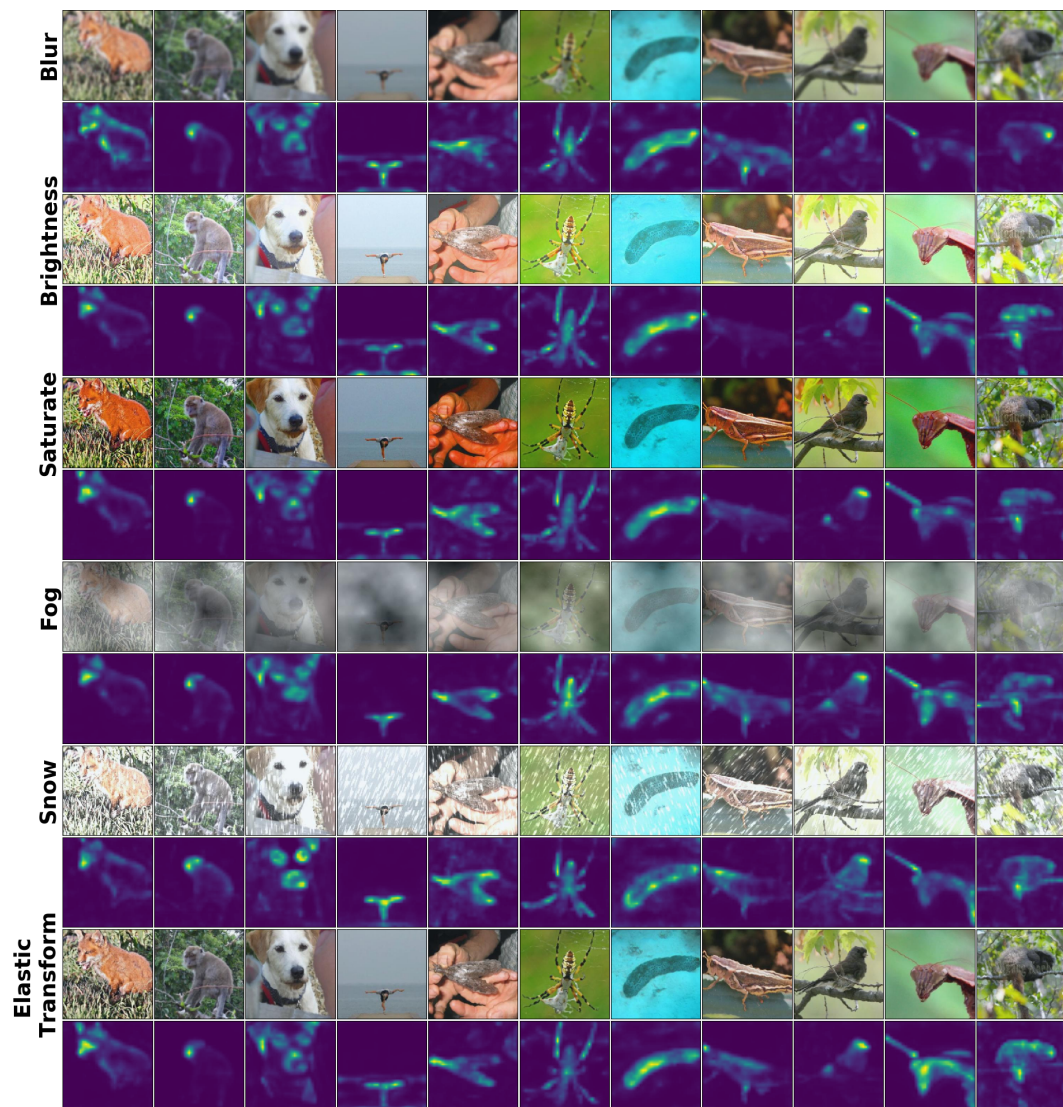


Figure 10: *Level-4* feature visualization from DGM ResNet-34 model under different color distortions (ImageNet-C). Note that our model is trained on the clean images from ImageNet dataset and is able to capture the object shape really well under challenging distortions.

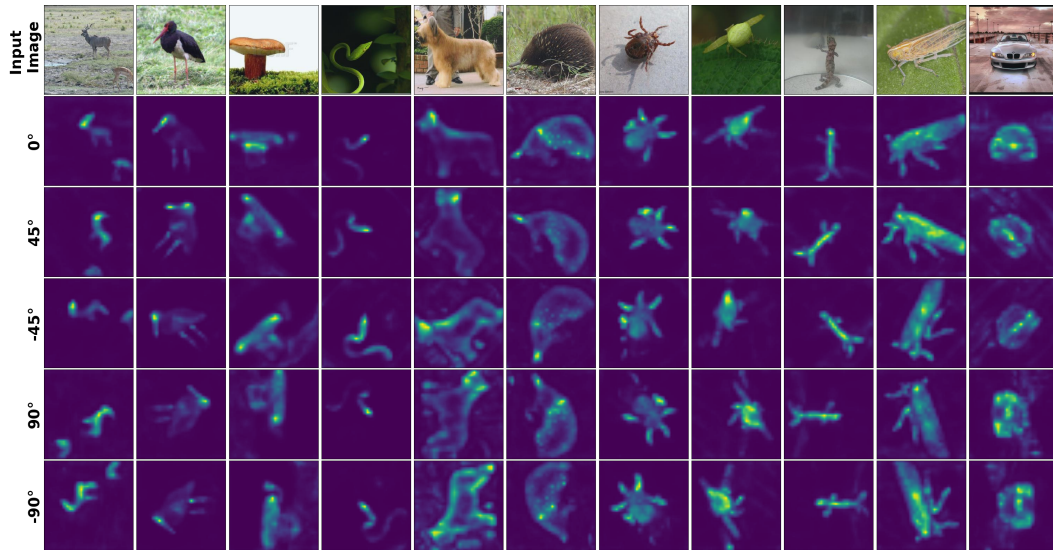


Figure 11: *Level-4* feature visualization from our DGM ResNet-34 model under different image rotation on ImageNet dataset. We do not use any affine transformation augmentation during training. Note the object shape is very well captured across different rotations of the image.

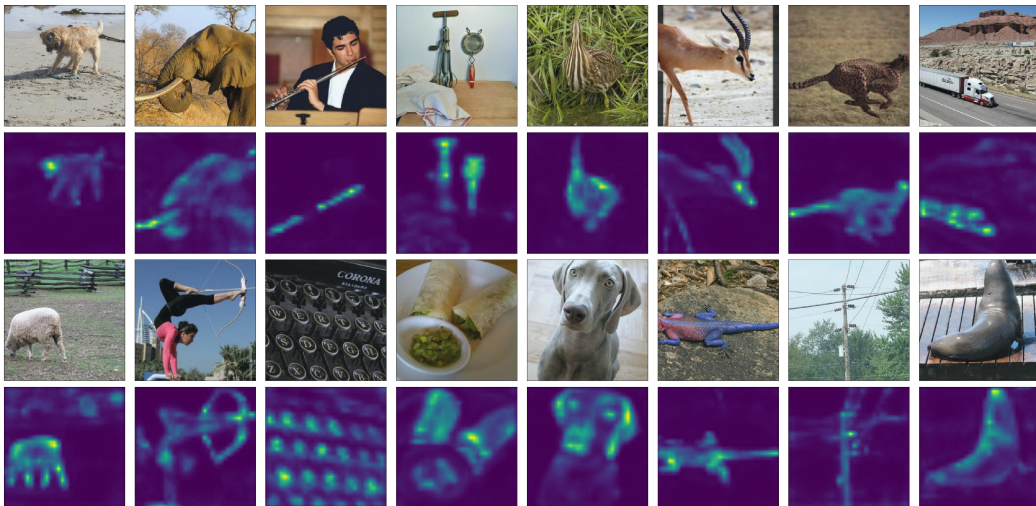


Figure 12: Few examples of *Level-4* feature visualization for DGM ResNet-34 model on the ImageNet dataset.